SPE 115790

Flow Rate Estimation From Wellhead Pressure and Temperature Data

B. Izgec, SPE, Chevron ETC; A.R. Hasan, SPE, U. of Minnesota-Duluth; D. Lin, North Dakota State U.; and C.S. Kabir, SPE, Chevron ETC

This paper was prepared for presentation at the 2008 SPE Annual Technical Conference and Exhibition held in Denver, Colorado, USA, 21–24 September 2008.

Abstract

Flow rate metering has less-than-satisfactory track record in the industry; modern sensors offer solution to this vexing problem. This paper offers two methods for estimating flow rates, predominantly from temperature data to complement rate measurements. One approach consists of modeling the entire wellbore and requires both wellhead pressure and temperature, whereas the other uses transient temperature formulation at a single point in the wellbore to compute the total production rate.

In the entire-wellbore approach, we use a wellbore model handling steady flow of fluids but unsteady-state heat transfer to estimate production rate, given wellhead pressure and temperature. The model rigorously accounts various thermal properties of the fluid and the formation, including Joule-Thompson heating and/or cooling. In the single-point approach, a single point temperature measurement made anywhere in the wellbore, including at the wellhead, is needed to estimate the mass rate at a given timestep. The method entails full transient treatment of the coupled fluid and heat flow problem at hand.

Examples from both gas and oil wells are shown to illustrate the application of the proposed methodology. Good correspondence between the measured and calculated results demonstrates the robustness of the proposed methods. These methods provide important rate information in various settings. For instance, in mature assets they can fill in the information void between tests or replace suspect rate data. Even well-instrumented wells can benefit because the methods can act as a verification tool, particularly in assets where integrated asset models are used to fine-tune rate allocation. In addition, the single-point approach can provide the much needed rate information during pressure-transient tests.

Introduction

Individual well rates enter into a variety of engineering calculations; paradoxically, the industry has struggled to meter this entity with decent accuracy. In fact, accuracy in flow metering has not kept pace with pressure and temperature measurements. Ordinarily, allocation algorithms are used to assign individual well rates from total production, unless a well is instrumented with a flowmeter. The lack of rigor of these allocation routines pose significant challenges during history matching of reservoir performance, particularly those involving rapidly changing events, such as coning or cresting of gas or water. In this context, test separators do not necessarily alleviate the metering issue simply because of inadequate flow time for large distances between a well and the point of separation, coupled with low-test frequency. To compound the matter further, the industry has lacked motivations for accurate metering of nonessential entities, such as water, and to a large extent gas because of its flaring in many field operations. In a case study, Kabir and Young (2002) discussed some of the issues related to gas and water metering in a typical brown-field operation.

To enhance the quality of rate measurements at the individual wells, dedicated metering has evolved over the past two decades. However, direct metering of multiphase fluid flow in a pipe is a difficult proposition because both volume fractions and the individual phase velocities must be ascertained. Accordingly, flowmeters have been developed to handle complete, partial, and no separation of phases. Because gas-volume fraction increases with decreasing pressure, downhole metering at higher pressures can largely mitigate handling of the gas phase. Venturi-type flowmeters, requiring no separation of phases, have gained wide acceptance both in downhole (Webster et al. 2006; Tibold et al. 2000; Brodie et al. 1995) and at surface (Warren et al. 2001, 2003; Retnanto et al. 2001; Pinguet et al. 2006). Venturi-type flowmeter appears to have performed well in a comparative study reported by Busaidi and Bhaskaran (2003). Like the venturi, downhole fiber-optic flowmeters is another nonintrusive device that has undergone considerable field testing (Kragas et al. 2002, 2003). Gas/Liquid Cylindrical Cyclone or GLCC technology (Kouba et al. 2006) separates gas from the liquid phases to facilitate ease of measurement at surface. The liquids are metered on the basis of mass using the Coriolis principle (Liu et al. 1988). Oglesby et al. (2006) reported their field experiences with GLCC while testing high-water-cut wells.

More recently, the increasing use of distributed temperature sensing or DTS has led to profiling flow across different producing intervals (Ouyang and Belanger 2006, Johnson et al. 2006, Wang et al. 2008). The knowledge of independent total rate at the wellhead allows appropriate zonal allocation of rate in accord with flow fraction. However, to our knowledge, estimation of total rate has not been demonstrated with temperature measurements alone. The intent of this work is to present two methods for estimating rates from temperature data, independent of flow sensing. The intrinsic idea is to provide engineering tools to check on measurement quality and fill in the information void where infrequent measurements are being made, such as in a brown-field environment.

Theoretical Development

We describe two methods for estimating rate. The first method involves the entire wellbore in that both pressure-drop and the attendant heat-transfer calculations are done. Here, the fluid flow occurs at steady state while unsteady-state heat flow occurs in the formation; this method is, therefore, designated as entire-wellbore approach. In the second method, we work with a single point in the wellbore by conserving mass, momentum, and energy in unsteady-state mode. This point may reside at any location in the wellbore where measurements occur, such as the wellhead. We term this approach as single-point method.

1. Enire-Wellbore Method. Our approach to estimating flow rate depends on the functional relationship between the production rate and the flowing-fluid temperature. Temperature difference between the wellbore fluid and its surrounding results in energy exchange. **Fig. 1** shows a typical offshore well with a number of changes in deviation angles and the temperature gradients for the surrounding.

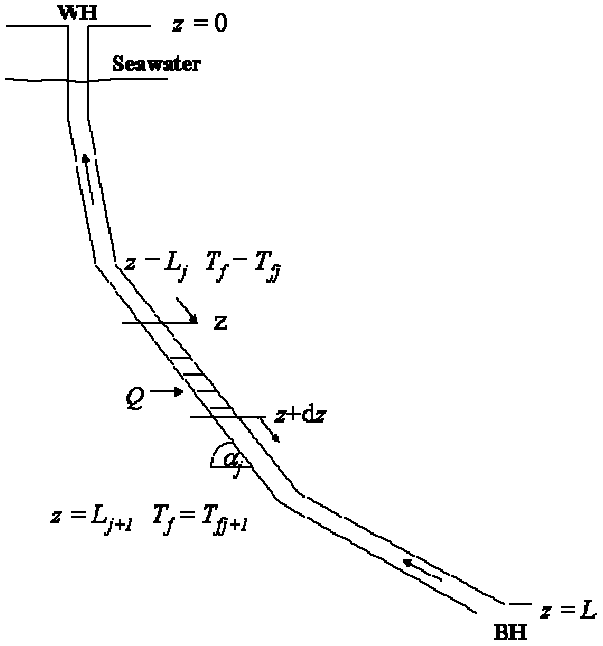

Fig. 1 – Wellbore schematic for energy balance.

Hasan *et al*. (2007) performed a general energy balance for the fluid, either single- or two-phase, to develop a first-order linear-differential equation describing the flow. With the boundary condition that fluid temperature at the measured distance, z_j; that is, the "entrance" to the section is known and is designated by T_{fj}, they developed the following analytic expression for fluid temperature

$$T_f = T_{ei} + \frac{1-e^{(z-z_j)L_R}}{L_R}\left[g_G \sin\alpha + \phi - \frac{g\sin\alpha}{c_p}\right] + e^{(z-z_j)L_R}\left(T_{f_j} - T_{ei\,j}\right) \quad \textbf{(1)}$$

For a wellbore section surrounded by earth, the relaxation distance, L_R, is given by the following expression:

$$L_R \equiv \frac{2\pi}{c_P w}\left[\frac{r_{to}U_{to}k_e}{k_e + (r_{to}U_{to}T_D)}\right] \quad \textbf{(2)}$$

where the dimensionless temperature function, T_D, is calculated from dimensionless producing time, t_D, using the following expression

$$T_D = \ln\left[e^{\left(-0.2t_D\right)} + \left(1.5 - 0.3719e^{-t_D}\right)\right]\sqrt{t_D} \quad \textbf{(3)}$$

For a wellbore section submerged in water, L_R is given by

$$L_{Rc} = \frac{2\pi r_{to}U_{toc}}{c_p w} \quad \textbf{(4)}$$

The dependence of fluid temperature on L_R, and, in turn, on mass rate, w, allows us to estimate the flow rate. Rewriting Eq. 1, we have

$$\left(T_f - T_{ei}\right) - e^{(z-z_j)L_R}\left(T_{f_j} - T_{ei\,j}\right) = \frac{1-e^{(z-z_j)L_R}}{L_R}\left[g_G \sin\alpha + \phi - \frac{g\sin\alpha}{c_p}\right] \quad \textbf{(5)}$$

For the usual case of a wellbore surrounded by earth, when Eq. 2 applies, the mass flow rate w is given by

$$w \equiv \frac{2\pi r_{to}U_{to}}{c_p}\left[\frac{k_e}{k_e+\left(r_{to}U_{to}T_D\right)}\right]\frac{1}{L_R} = \frac{2\pi r_{to}U_{to}}{c_p}\left[\frac{k_e}{k_e+\left(r_{to}U_{to}T_D\right)}\right] f(T) \quad \textbf{(6)}$$

For the submerged section of an offshore well, when Eq. 4 applies, the term in the bracket in Eq. 6 is replaced by 1, leading to

$$w = \frac{2\pi r_{to}U_{to}}{c_P} f(T) \quad \textbf{(7)}$$

In both Eqs. 6 and 7, the temperature function, $f(T)$, is given by

$$f(T) = \frac{\left(T_f - T_{ei}\right) - e^{(z-z_j)L_R}\left(T_{f_j} - T_{ei\,j}\right)}{\left(1-e^{(z-z_j)L_R}\right)\left(g_G \sin\alpha + \phi - \frac{g\sin\alpha}{c_p}\right)} \quad \textbf{(8)}$$

Note that the values of the parameters, T_{ei}, g_G, ϕ, α, etc., to be used in Eq. 1 are those that apply to this section. Among these, ϕ lumps kinetic energy with the Joule-Thompson (Thompson and Joule 1853) or J-T coefficient, and is given by

$$\phi = \frac{v}{c_p J g_c}\frac{\mathrm{d}v}{\mathrm{d}z} - C_J\frac{\mathrm{d}p}{\mathrm{d}z} \quad \textbf{(9)}$$

Expressions for Thermodynamic Parameters. The use of Eq. 6 or 7, along with Eq. 8, requires an estimate of ϕ. Because ϕ is the sum of kinetic energy and J-T terms, a single empirical expression for it may lead to unacceptable errors. Many modern wells produce at very high rates, thereby making contribution of the kinetic energy term in ϕ significant. Large pressure gradients associated with high-production rates also exacerbate the J-T effect. Additionally, not only is the J-T effect in low-pressure gas wells opposite to that of oil wells, the J-T effect in high-pressure gas wells is usually opposite to that in low-pressure gas wells (Ayala 2007, Hasan et al. 2007).

These thermodynamic considerations led us to evaluate the two terms in ϕ individually. Noting that for either single- or two-phase flow, c_pC_J is given by $-[V-T(\partial V/\partial T)_P]$, Hasan *et al.* (2007) presented the following general expression for the J-T coefficient:

$$C_J c_p = \frac{xT}{ZM_g \rho_g}\left(\frac{\partial Z}{\partial T}\right)_p - (1-x)\frac{1-T\beta}{\rho_L} \quad \textbf{(10)}$$

where Z is the gas compressibility factor ($\equiv VpM_g/RT$) and β is the liquid-volume expansivity, which is given by

$$\beta \equiv (1/V)(\partial V/\partial T)_p \equiv (-1/\rho)(\partial \rho/\partial T)_p \quad \textbf{(11)}$$

Solution Algorithm. Examination of either Eq. 6 or Eq. 7 reveals that the expression is implicit in rate because $f(T)$ on the right side of Eq. 6 contains L_R, which requires knowledge of w. Because w appears on both sides of the equations, an iterative solution approach is called for. We start with a trial value of L_R, use Eq. 7 to estimate $f(T)$, estimate w from either Eq. 6 or Eq. 7, and recalculate L_R from Eq. 2 or Eq. 4. This process is repeated until two subsequent values of L_R are within a specified tolerance.

During steady-state production, the mass flow rate passing through each point is the same. Nonetheless, properties, such as geothermal gradient, number of casings, cement thickness, heat capacity, and thermal conductivity of the formation are different throughout the wellbore. For a simple well with a single deviation angle and geothermal gradient, the approach mentioned above can be directly used to iteratively calculate flow rate from wellhead data. However, as Hasan *et al.* (2007) pointed out, most wells traverse multiple geothermal gradients with varying deviation angles. Our heat transfer modeling, therefore, discretizes the wellbore into a number of sections. Let us presuppose that BHT, WHT, and WHP are known; however, neither the entire fluid temperature profile nor the BHP data are available. Computations start from the bottomhole assuming a rate and a BHP, leading to T_f estimation at a node above the bottomhole using Eq. 1, and computation continues until the wellhead is reached. Differences in the calculated WHT and WHP with the measured data are used to estimate improved values of rate and BHP. The process is continued until an acceptable accuracy is attained.

Calculating an accurate pressure profile is as important as an accurate temperature profile because of their coupled nature. This fact becomes evident when one computes the J-T coefficient and ϕ value at each cell. For instance, a slightly erroneous value of C_J, which depends on pressure, will cause poor estimation of ϕ, leading to a significant error in the estimated temperature. An important lesson learned from these calculations is that a bottom-up computational approach is much superior to a top-down approach. Starting from the wellhead with an inaccurate set of data usually leads to increasing errors at each cell, with a strong tendency to diverge from the true solution. Calculations starting from the bottomhole usually converge quickly.

2. Single-Point Method. Fluid production through the tubing creates a unique temperature profile at every depth in the wellbore during each timestep. At a given point in the wellbore, amounts of heat brought from the reservoir and lost to the surroundings determine the changes in fluid temperature as a function of time. Under any production- and/or well-configuration scenario, the total production rate is the major contributor for the changes in temperature. At any point in the wellbore, this unique temperature profile can be traced back to the total amount of fluid passing through that single point, given that the physical description of the system is within engineering accuracy. We used a methodology that minimizes the difference between measured and model calculated temperature values by continuously iterating on the mass flow rate. The Newton-Raphson method for mass flux calculation at a single point is defined as

$$w_{l+1}^{k} = w_{l+1}^{k-1} - \frac{R_{l+1}^{k-1}}{\left(\partial R_{l+1}^{k-1} / \partial w_{l+1}^{k-1}\right)} \quad \textbf{(12)}$$

where "w" is the total production rate in lbm/hr. The subscript "l+1" stands for new time level and "k" represents the iteration number. The algorithm calculates the mass flow rate and uses it to generate temperature profiles through a temperature model. "R" is defined as a residual function and is given by

$$R = T_{fc} - T_{fm} \quad \textbf{(13)}$$

The residual function is the temperature difference between the computed value, T_{fc}, and measured data, T_{fm}. Iteration continues until a satisfactory match is obtained between the two temperature values or the residual function is very close to zero. The derivative of the residual function with respect to mass flux rate at a given timestep is given as

$$\frac{\partial R_{l+1}^{k-1}}{\partial w_{l+1}} = \frac{\partial}{\partial w_{l+1}}\left[T_{fc} - T_{fm}\right]_{l+1} \quad \textbf{(14)}$$

Expanding,

$$\frac{\partial R_{l+1}^{k-1}}{\partial w_{l+1}} = \frac{\partial T_{f\,c}}{\partial w_{l+1}} - \frac{\partial T_{f\,m}}{\partial w_{l+1}} \quad \textbf{(15)}$$

The second term on the right-hand side drops out because field data are not affected by model-generated mass fluxes. The expression for the residual function then becomes

$$\frac{\partial R_{l+1}^{k-1}}{\partial w_{l+1}} = \frac{\partial T_{f\,c}}{\partial w_{l+1}} \quad \textbf{(16)}$$

The derivative of model calculated temperatures with respect to mass flux can be taken either numerically or analytically. The numeric expression can be shown as

$$\frac{\partial T_{f\,c}}{\partial w_{l+1}} = \frac{T_f^{\,k} - T_f^{\,k-1}}{w_{l+1}^{k} - w_{l+1}^{k-1}} \quad \textbf{(17)}$$

The analytic derivative is dependent upon the temperature model employed. We used the following analytic temperature model (Hasan *et al*. 2005, Izgec *et al*. 2007a).

$$T_f = T_{ei} + \frac{1 - e^{-aL_R t}}{L_R}\left[1 - e^{(z-L)L_R}\right]\psi \quad \textbf{(18)}$$

The derivative of temperature model with respect to current time step mass flux rate becomes

$$\frac{\partial T_{f\,c}}{\partial w_{l+1}} = \frac{\partial}{\partial w_{l+1}}\left[T_{ei} + \frac{1 - e^{-aL_R t}}{L_R}\left[1 - e^{(z-L)L_R}\right]\psi\right] \quad \textbf{(19)}$$

In Eq. 18, "*a*" is defined in terms of fluid mass in control volume per unit length ($m = \rho_f \pi r_t^{\,2}$) and the thermal-storage parameter C_T (Hasan et al. 2005), as

$$a = \frac{w}{m(1 + C_T)} \quad \textbf{(20)}$$

The thermal-storage parameter value depends on actual wellbore material and is usually 3 for drawndown and 2 for buildup. The term Ψ in Eq. 18 lumps the geothermal gradient, ϕ, defined by Eq. 9, and the static head as follows:

$$\psi = g_G \sin\theta + \phi - \frac{g \sin\theta}{J g_c c_p} \equiv g_G \sin\theta + \phi - \frac{\sin\theta}{778.16\, c_p} \quad \textbf{(21)}$$

The final form of the analytic derivative of temperature model with respect to mass flux is

$$\frac{\partial T_{f\,c}}{\partial w_{l+1}} = \frac{1-e^{-a\,L_R\,t}}{L_R{}'}\left[1-e^{(z-L)L_R}\right]\psi \qquad (22)$$

and

$$L_R{}' = w\,L_R \qquad (23)$$

The analytic derivative of the residual function is

$$\frac{\partial R^{k-1}_{l+1}}{\partial w_{l+1}} = \frac{1-e^{-a\,L_R\,t}}{L_R{}'}\left[1-e^{(z-L)L_R}\right]\psi \qquad (24)$$

Note that this analytic derivative is not precise because of the complicated nature of the temperature model. In particular, the exponential terms include mass flux rate at current time step. But the iterative nature of the solution compensates for the lack of a complete differentiation with respect to mass flux rate. However, numeric derivative may also be employed to accelerate the convergence.

Calculation Algorithm. In this approach, we initially assume a mass rate at a given timestep, and then the fluid temperature is estimated with Eq. 18. Knowing the measured fluid temperature, $T_{fm,}$ and computed fluid temperature, T_{fc}, the residual function is evaluated with Eq. 13. Thereafter, either the numeric (Eq. 17) or the analytic derivative (Eq. 24) of the residual function is evaluated. Mass flux is then estimated with Eq. 12, followed by the fluid temperature estimation with the new mass rate. This process is repeated until convergence is attained within a specified tolerance.

Example Applications

In this section we present four examples. First, we generate a flow problem using a forward simulator (Izgec, et al. 2007a) and analyze with the unsteady-state approach to prove that the proposed methodology works in principle. Thereafter, three field examples show applications of both the entire-wellbore and single-point methods.

1. Synthetic example for proof of concept. Consider production of single-phase oil from a 26,400 ft well. Temperature measurements are made at three locations, as shown in **Fig. 2,** corresponding to an imposed variable-rate history. Our objective is to reproduce the imposed rate profile, regardless of temperature measurements made at any point in the wellbore. Note that Fig. 2 also presents the computed temperature en route to computing the rate history. **Fig. 3** presents the rate match at 16,000 ft. As expected the same quality match is attained at other stations for the same flow problem at hand.

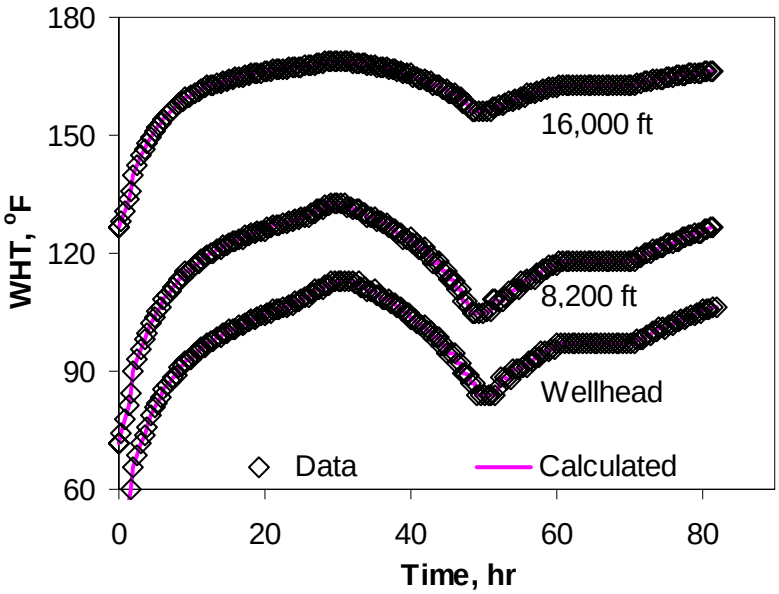

Fig. 2 – Matching fluid temperature at various well depths.

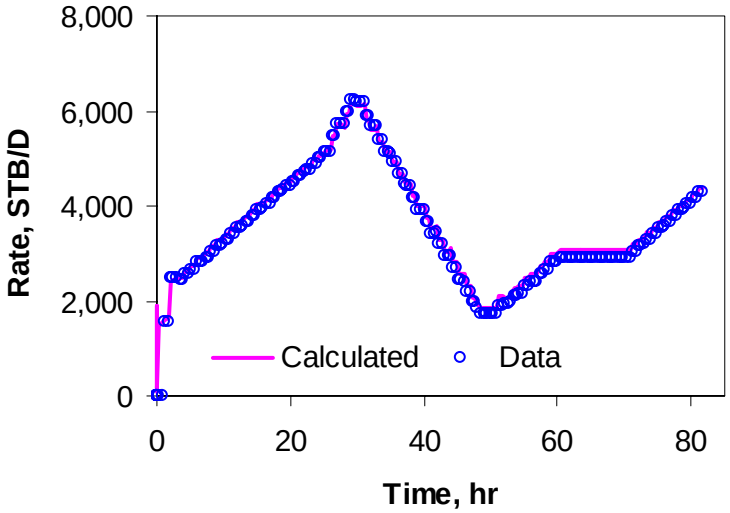

Fig. 3 – Computed rate at 16,000 ft reproduces the input model rate profile.

2. Multirate gas-well test example. This example comes from a vertical gas well in a high-temperature reservoir, located in the US Gulf Coast (Kabir et al. 1996). Pressure and temperature data were available both at bottomhole and wellhead from a multirate test. **Fig. 4** shows that the transient wellhead temperature was matched with the single-point method en route to computing rate. **Fig. 5** compares and contrasts the measured rates with those obtained from the two computational methods. One important difference between the entire-wellbore and single-point methods is that the transient nature of rate is captured by the latter. We think this is a significant development in that even many surface sensors may not be able to capture subtle rate variation during a transient test. Put another way, the ever-changing rate, which is a direct reflection of temperature, suggests dominanting wellbore storage effect in this 20,000-ft well with 0.35 md formation permeability.

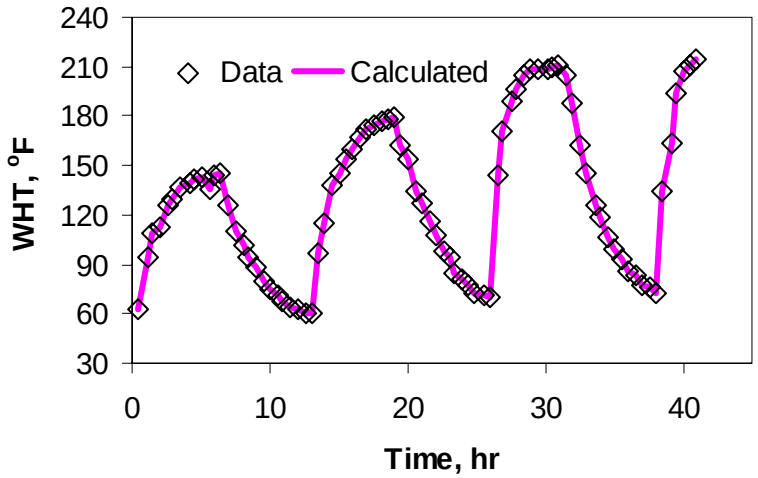

Fig. 4 – Matching WHT with single-point approach.

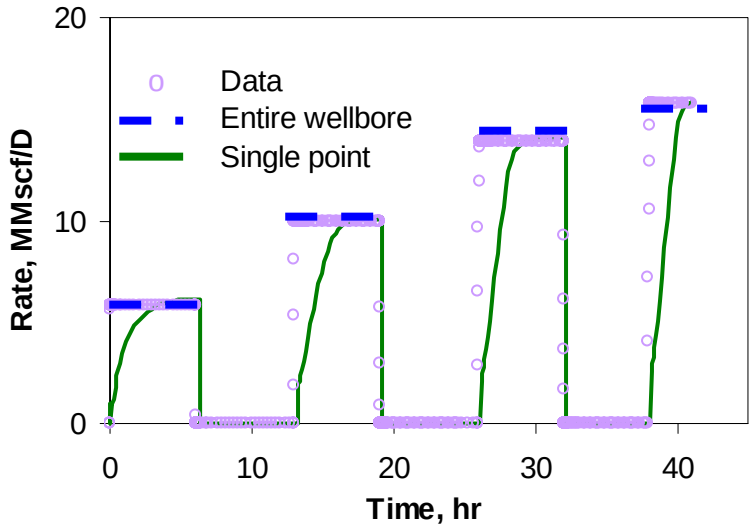

Fig. 5 – Comparing measured and computed rates with both methods.

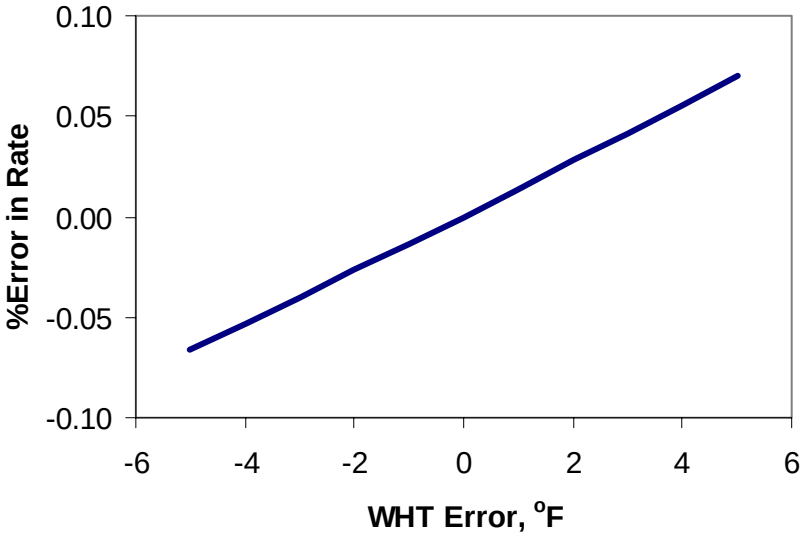

Fig. 6 – How WHT error manifests in rate calculation uncertainty.

Questions arise about the quality of rate solution. We investigated the sensitivity of estimated flow rate with the entire-wellbore modeling approach. To illustrate the effect of temperature error on rate calculations, we considered the recorded wellhead temperature for the second rate period involving 10 MMscf/D. **Fig. 6** shows that the proposed method is quite robust. Indeed, rate estimation is not very sensitive to wellhead temperature; an error of 5 °F in WHT leads to a 7% error is estimated rate.

3. Gas-well test with wellbore temperature profile. This 7000-ft dry gas well is vertical for the first 2,500 ft and deviates thereafter by 50° from vertical, terminating at a TVD of 5,412 ft. At a reported production rate of 50 MMscf/D, the WHT and BHT are 129 °F and 150 °F, respectively. A production log was also run, thereby providing us with a distributed-temperature profile throughout the wellbore. Because steady flow was prevalent for 48 hours, we invoked the entire-wellbore modeling approach. With three iterations the model estimated a rate of 49.7 MMscf/D, which is in good agreement with the data. **Fig. 7** depicts the temperature-profile match obtained during history matching.

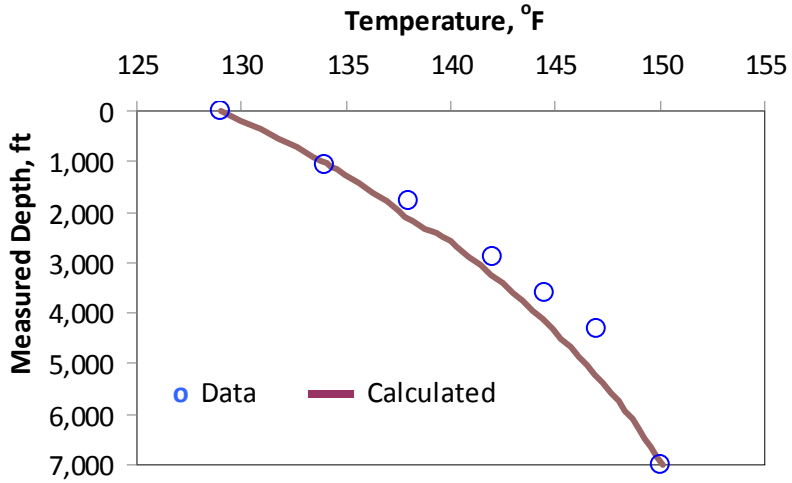

Fig. 7 – Wellbore temperature profile match obtained en route to rate estimation with entire-wellbore approach.

We solved the same problem with the single-point approach. At each station the same rate of 50 MMscf/D was calculated. However, we observed that the absolute error in the computed fluid temperature had an increasing trend with increasing depth. In particular, at the last station, the error is 1.63 °F, as **Fig. 8** indicates. We think that this error is triggered by the diminished perturbation in measured temperature owing to significant decrease in heat transfer as the station approaches the producing interval. Nonetheless, if a permanent sensor is located too close to the producing interval, we can easily calibrate the model with a known rate measurement to allow accurate estimation at other flow conditions.

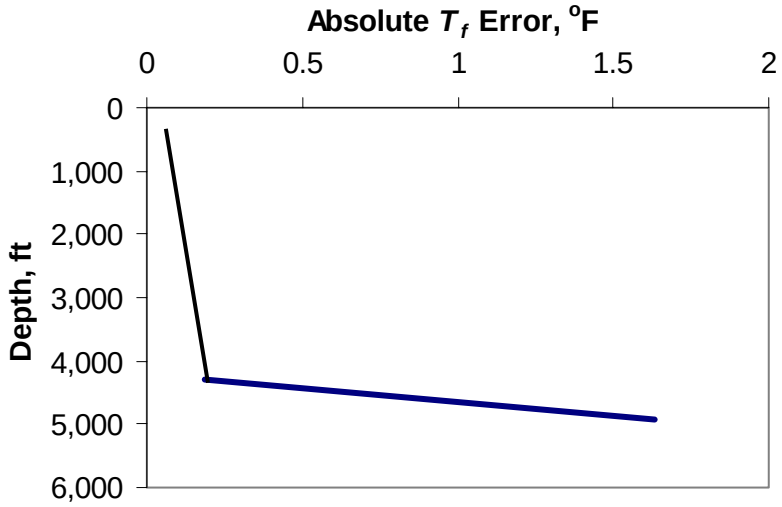

Fig. 8 – Error in fluid temperature estimation at each station with single-point approach.

4. Tahiti multirate oil-well test. This field example was discussed earlier by Izgec et al. (2007b). In this deepwater setting, a combined cleanup and shut-in period of about 70 hours preceded the variable-rate test, lasting about 60 hours. A shut-in test followed, thereafter. Because of the transient nature of the flow problem, we invoked the single-point approach in estimating rate. **Fig. 9** depicts the temperature data measured at 9,600 ft MD; the reservoir depth occurs at 26,500 ft MD. Also shown in Fig. 8 is the quality of temperature match, en route to computing the rate history. **Fig. 10** compares and contrasts the computed rate history with that measured at surface. Overall, the match appears good with the exception of those occurring at the highest rates. Physical limitations of rate metering capability at surface required that the rate in excess of 9,000 STB/D be diverted to another vessel. Issues with metering at the secondary facility precipitated the discrepancy in rate.

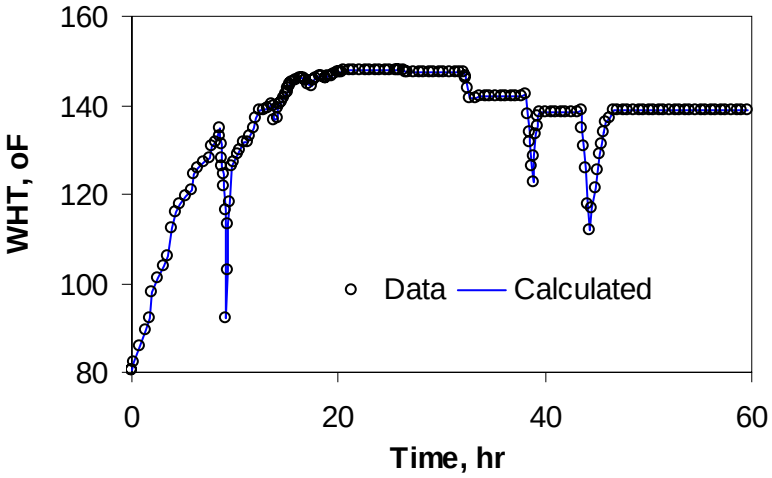

Fig. 9 – Matching cell temperature at 9,600 ft MD.

Let us explore how the computed rate history impacts the pressure-buildup analysis that followed the 60-hr flow period, discussed earlier by Izgec et al. (2007b). The maximum discrepancy in rate is about 16% occurring at about 25 hr. Because the point of discrepancy occurs at a distant past relative to the buildup test, the error in the permeability-thickness product, *kh,* turns out to me minimal; only 2% lower than that estimated previously. However, had this rate discrepancy occurred just preceding the buildup test, the magnitude of error in *kh* estimation would have been directly proportional to the rate itself. This example underscores the importance of validating rate history prior to doing any transient analysis. Matching data at both ends of the peak rates provides confidence in our ability to compute rate from temperature measurements at any point in the wellbore.

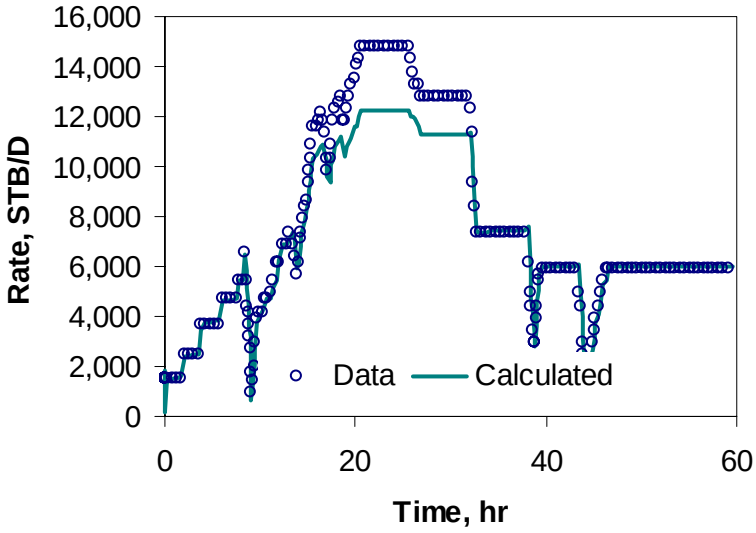

Fig. 10 – Computed oil rate compares favorably with measured values.

Discussion

In this study, we have verified both methods with example applications. The two methods offer relative strengths, however. In the entire-wellbore approach, the tubular and cement sheath dimension, together with fluid, tubular, and formation thermal

properties are needed as input parameters. Because the method relies upon modeling fluid and heat flows in the entire wellbore, both wellhead pressure and temperature are required. In this method, the entire wellbore is modeled in a bottom-up mode, en route to seeking convergence with WHT and WHP, thereby instilling confidence in the solutions. By contrast, the single-point method is more flexible in that it requires only the temperature measurement at any point in the wellbore, plus the attendant fluid and thermal properties of the media at that point. Of course, the method needs the overall-heat-transfer coefficient at the point of temperature measurement and is evaluated with an iteravtive scheme, as discussed in Appendix A. Because this method relies on a point measurement, the approach offers the advantage of being applicable in a large variety of well completion and instrumentation.

In their current formulations, both methods presuppose that wellbore fluid and thermal storage effects are minimal. These conditions are well satisfied in single-phase flow in high-permeability-thickness (*kh*) reservoirs, particularly for the single-point method. Tahiti example satisfies this condition rather well and so does the synthetic example illustrating method's ability to capture rate transients solely from temperature measurements. However, in a low-*kh* reservoir with long compressible-fluid column, thermal transients may outlast fluid-storage effects, leading to apparently long time for the rate stabilization to occur. This point is illustrated by the Gulf Coast gas example where the low-*kh* formation and 20,000-ft wellbore triggers a rather long stabilization time. In contrast, the other gas example with distributed-temperature measurement exhibits rapid rate stabilization owing to high-*kh* formation.

Potential applications of either method span a large spectrum of situations. For instance, rate allocation has a large uncertainty bar in most business settings; either method can work well after calibration is attained with dedicated well measurements. Many well completions prevent placement of permanent sensors close to perforations. In this setting, the single-point method offers an opportunity to capture rate because off-bottom measurements will afford significant heat transfer between the wellbore fluid and the formation, leading to significant temperature perturbation. While such off-bottom measurements pose challenge in estimating formation parameters with pressure-transient analysis (Izgec et al. 2007b), they offer a better opportunity for estimating rate. Exploration-well testing is another area where the single-point method appears particularly appealing; the Tahiti test is a case in point. In all cases, we view the proposed methods to be complementary to conventional metering.

Conclusions

1. This study presents two independent methods for computing rate, predominantly from temperature measurements. In the entire-wellbore approach, both WHT and WHP are matched en route to estimating flow rate. In contrast, the single-point method works off of temperature measured at any point in the wellbore.
2. Field data corroborates the estimated rates for both gas and oil wells. Limited computational results suggest that the single-point method is capable of capturing transient rates, provided fluid and thermal storage effects are minimal at the point of interest.
3. The proposed methods provide a vital tool for checking rates even in well-instrumented systems, without any overhead.

Acknowledgment

We appreciate input of many colleagues for providing the field data and thank Chevron management for permission to publish this work.

Nomenclature

a = thermal parameter defined by Eq. 19, ft/hr
c_p = specific heat capacity of fluid, Btu/lbm-^{o}F
C_J = Joule-Thompson coefficient, (^{o}F)/(lb$_f$/ft^2)
C_T = Thermal storage parameter, dimentionless
g = gravitational acceleration, ft/sec^2
g_c = conversion factor, 32.17 lbm-ft/lbf/sec^2
g_G = geothermal gradient, ^{o}F/ft
h = formation thickness, ft
H = fluid enthalpy, Btu/lbm
J = Btu to ft-lbf conversion factor
k = formation permeability, md
k_a = thermal conductivity of annular fluid, Btu/hr-ft-^{o}F
k_e = thermal conductivity of earth, Btu/hr-ft-^{o}F
L_R = relaxation parameter defined by Eq.A-2 or A-3, ft^{-1}
L = measured depth of wellbore, ft
L_j = measured (from wellhead) depth of section 'j' of wellbore, ft
m = mass of fluid, lbm
M_g= molecular weight of the free gas, lbm/lb mole
p = pressure, psi

q_o = oil flow rate, STB/D
Q = heat flow rate per unit length of wellbore, Btu/hr/ft
r_w = wellbore radius, ft
R = residual, defined by Eq. 13, °F
s = mechanical skin, dimensionless
t = producing time, hr
t_D = dimensionless time, hr
T_D = dimensionless temperature
T_e = earth or formation temperature, °F
T or T_f = fluid temperature, °F
T_{fc} = computed fluid temperature, °F
T_{fm} = measured fluid temperature, °F
T_{ei} = undisturbed earth or formation temperature, °F
T_{wb} = wellbore/earth interface temperature, °F
U_{to} = overall-heat-transfer coefficient, Btu/hr-ft^2-°F
v = velocity, ft/s
V = fluid specific volume (=1/ ρ), ft^3/lbm
w = mass rate, lbm/hr
x = gas mass fraction (quality), dimentionless
z = variable well depth from surface, ft
Z = gas compressibilty factor, dimentionless
α = well inclination (to horizontal) angle, degree
β = volume expansivity, °F^{-1}
γ_o = oil gravity, °API
γ_g = gas gravity (air = 1), dimensionless
μ = fluid viscosity, cp
ρ = fluid density, lbm/ft^3
ρ_e = earth or formation density, lbm/ft^3
ϕ = lumped parameter defined by Eq. 9, °F/ft
σ = standard deviation of pressure, psi
ψ = $g_G sin\theta + \phi - (g sin\theta / c_p J g_c)$, °F/ft
θ = well deviation from vertical, degree

Subscripts

c = calculated
e = earth (formation)
ei = initial earth contion (for temperature)
f = fluid
l = time step
m = measured

References

Ayala H., L.F. 2006. On the Non-Ideality of Hydrocarbon Fluids: Implications for Natural Gas Engineering–Part B, *Petroleum Journals Online,* **1** (1): 1–9.

Brodie, A.D., Allan, J.C., and Hill, G. 1995. Operating Experience With ESP's and Permanent Downhole Flowmeters in Wytch Farm Extended-Reach Wells. *JPT* **47** (10): 902–906.

Busaidi, K. and Bhaskaran, H. 2003. Multiphase Flow Meters: Experience and Assessment in PDO. Paper SPE 84505 presented at the SPE Annual Technical Conference and Exhibition, Denver, Colorado, 1–4 October.

Hasan, A.R., Kabir, C.S., and Wang, X. 2007. A Robust Steady-State Model for Flowing-Fluid Temperature in Complex Wells. Paper SPE 109765 presented at the SPE Annual Technical Conference and Exhibition, Anaheim, California, 11–14 November; to appear in *SPEPO.*

Hasan, A.R., Kabir, C.S., and Lin, D. 2005. Analytic Wellbore-Temperature Model for Transient Gas-Well Testing. *SPEREE* **8** (3): 240–247.

Izgec, B., Kabir, C.S., Zhu, D., and Hasan, A.R. 2007a. Transient Fluid and Heat Flow Modeling in Coupled Wellbore/Reservoir Systems. *SPEREE* **10** (3): 294–301.

Izgec, B., Cribbs, M.E., Pace, S., Zhu, D., and Kabir, C.S. 2007b. Placement of Permanent Downhole Pressure Sensors in Reservoir Surveillance. Paper SPE 107268 presented at the SPE Europec/EAGE Annual Conference and Exhibition, London, United Kingdom, 11–14 June.

Johnson, D., Sierra, J., Kaura, J., and Gualtieri. 2006. Successful Flow Profiling of Gas Wells Using Distributed Temperature Sensing Data. Paper SPE 103097 presented at the SPE Annual Technical Conference and Exhibition, San Antonio, Texas, 24–27 September.

Kabir, C.S. and Young, N.J. 2004. Handling Production-Data Uncertainty in History Matching: The Meren Reservoir Case Study. *SPEREE* **7** (2): 123–131.

Kabir, C.S., Hasan, A.R., Jordan, D.L., and Wang, X. 1996. A Transient Wellbore/Reservoir Model for Testing Gas Wells in High-Temperature

Reservoirs. *SPEFE* **11** (2): 128–134.
Kouba, G.E., Wang, S., Gomez, L., Mohan, R., and Shoham, O. 2006. Review of the State-of-the-Art Gas/Liquid Cylindrical Cyclone (GLCC) Technology—Field Applications. Paper SPE 104256 presented at the SPE International Oil & Gas Conference and Exhibition, Beijing, China, 5–7 December.
Kragas, T.K., van der Spek, A., and Al-Hashmi, K.M. 2002. Field Trial of a Downhole, Fiber Optic, Two-Phase Flowmeter in PDO's Nimr Field. Paper SPE 78306 presented at the SPE European Petroleum Conference, Aberdeen, Scotland, 29–31 October.
Kragas, T.K., Johansen, E.S., Hassanali, H., and Da Costa, S.L. 2003. Installation and Data Analysis of a Downhole, Fiber Optic Flowmeter at Mahogany Field, Offshore Trinidad. Paper SPE 81018 presented at the SPE Latin American and Caribbean Petroleum Engineering Conference, Port-of-Spain, Trinidad and Tobago, 27–30 April.
Liu, K.T., Canfield, D.R., and Conley, J.T. 1988. Application of a Mass Flowmeter for Allocation Measurement of Crude Oil Production. *SPEPE* **3** (4): 633–636.
Oglesby, K.D., Mehdizadeh, P., and Rodger, G.J. 2006. Portable Multiphase Production Tester for High-Water-Cut Wells. Paper SPE 103087 presented at the SPE Annual Technical Conference and Exhibition, San Antonio, Texas, 24–27 September.
Ouyang, L-B. and Belanger, D. 2006. Flow Profiling by Distributed Temperature Sensor (DTS) System–Expectation and Reality. *SPEPO* **21** (2): 269–281.
Pinguet, B.G., Roux, G., and Hopman, N. 2006. Field Experience in Multiphase Gas-Well Testing: The Benefit of the Combination of Venturi and Gamma Ray Fraction Meter. Paper SPE 103223 presented at the SPE Annual Technical Conference and Exhibition, San Antonio, Texas, 24–27 September.
Ramey, H.J., Jr. 1962. Wellbore Heat Transmission. *JPT* **14** (4): 427–435.
Retnanto, A. et al. 2001. Production Optimization Using Multiphase Well Testing: A Case Study From East Kalimantan, Indonesia. Paper SPE 71534 presented at the SPE Annual Technical Conference and Exhibition, New Orleans, Louisiana, 30 September–3 October.
Thompson, W. and Joule, J.P. 1853. On the Thermal Effects of Fluids in Motion. *Philosophical Transactions of the Royal Society of London.* **143**: 357–365.
Tibold, M.P., Simonian, S., Chawla, M., and Akbar, M. 2000. Well Testing With a Permanent Monitoring System. Paper SPE 63079 presented at the SPE Annual Technical Conference and Exhibition, Dallas, Texas, 1–4 October.
Wang, X., et al. 2008. Modeling Flow Profile Using Distributed Temperature Sensor (DTS) System. Paper SPE 111790 presented at the SPE Intelligent Energy Conference and Exhibition, Amsterdam, The Netherlands, 25–27 January.
Warren, P.B., Hussain, S., and Ghamdi, S. 2001. Background and Operational Experience of Multiphase Metering in the Safaniya Field—Offshore Saudi Arabia. Paper SPE 71534 presented at the SPE Annual Technical Conference and Exhibition, New Orleans, Louisiana, 30 September–3 October.
Warren, P.B., et al. 2003. Field Testing a Compact Multiphase Flow Meter—Offshore Saudi Arabia. Paper SPE 81560 presented at the SPE Middle East Oil Show and Conference, Mahrain, 5–8 April.
Webster, M., et al. 2006. Well Surveillance With a Permanent Downhole Multiphase Flowmeter. *SPEPO* **21** (3): 388–393.

Appendix A – Estimating Upper and Lower Limits of Overall-Heat-Transfer Coefficient

This section provides a simple diagnostic plot to estimate the range of overall-heat-transfer coefficient (U_{to}) by graphing the model-generated-mass-flux rates with changes in fluid temperature relative to the initial condition at the point of interest. This method is illustrated by generating the mass rate versus temperature difference plot for the Tahiti well example.

In this particular case, data collection point was located about 1,000 ft below a salt feature with a complex completion scheme consisting of multiple sealed annuli and vacuum-insulated tubing to prevent annulus-pressure buildup. The resistances offered by multiple annuli and their trapped fluid, vacuum insulated tubing, and the presence of thick salt layer makes theoretical estimation of the overall-heat-transfer coefficient difficult. **Fig. A-1**, which is generated with an U_{to} of 1.0 Btu/hr-ft^2-^{o}F, suggests that the heat-transfer rate from the tubing fluid to the formation does not reach steady-state even after 60 hours of production. This conclusion can be supported by lack of any identifiable relationship between the mass flux and temperature difference.

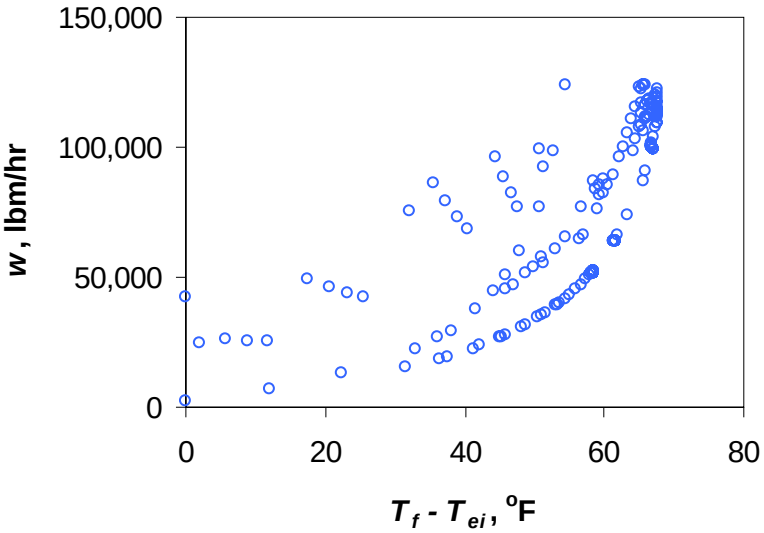

Fig. A1 – Inappropriate U_{to} value of 1.0 produces data scatter.

Fig. A2, on the other hand, displays a straight line at late times with U_{to} of 1.85 Btu/hr-ft^2-°F. This straight line signifies an established relationship between mass flux rate and change in fluid temperature at the measurement depth. As shown earlier in Fig. 9, this U_{to} value provided the best match between the field reported and model generated rates. In this case, the early-time scatter disappears after 14 hours, as **Fig. A3** demonstrates.

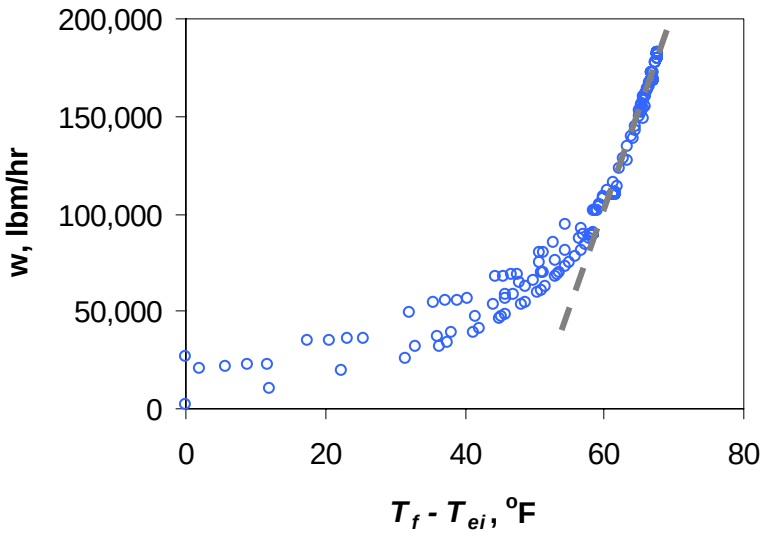

Fig. A2 – U_{to} value of 1.85 produces the expected trend at late times.

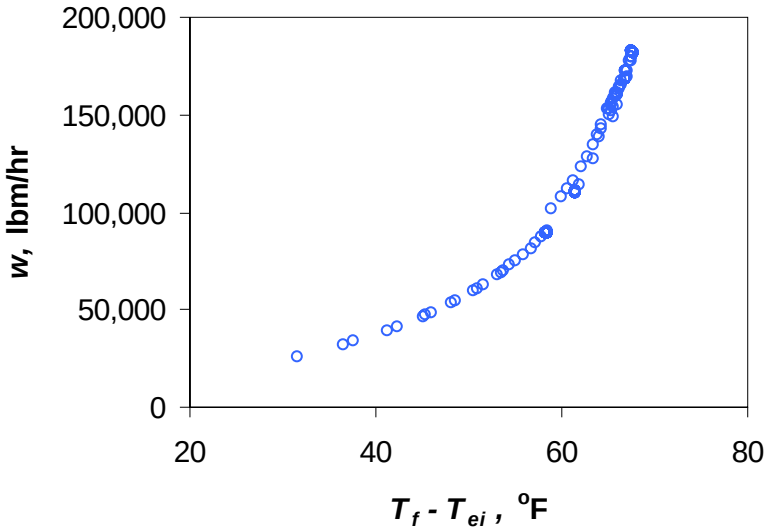

Fig. A3 – Less ambiguous rate/temperature-difference relationship emerges after 14 hours.

We derive our support of the preceding observations by investigating the equation proposed by Ramey (1962) for steady-state heat transfer, which is given by

$$\frac{dT}{dz} = -(T_{ei} - T_f)L_R \qquad \textbf{(A-1)}$$

By using the definition of relaxation-distance parameter, L_R, given in Eq. 2, we can rewrite Eq. A-1 as

$$\frac{dT}{dz} = -(T_{ei} - T_f)\frac{2\pi}{wc_p}\left[\frac{r_{to}U_{to}k_e}{k_e + r_{to}U_{to}T_D}\right] \qquad \textbf{(A-2)}$$

Manipulating,

$$w\ \frac{dT}{dz}\frac{k_e + r_{to}U_{to}T_D}{r_{to}U_{to}k_e}\ \frac{c_p}{2\pi} = (T_f - T_{ei}) \qquad \textbf{(A-3)}$$

All the parameters on the left-hand side, excluding mass-flow rate, can be lumped together as

$$C = \frac{dT}{dz}\frac{k_e + r_{to}U_{to}T_D}{r_{to}U_{to}k_e}\ \frac{c_p}{2\pi} \qquad \textbf{(A-4)}$$

Because the methodology for temperature difference to mass-flow rate relationship is applied to a single point in the wellbore, the derivative of temperature value with respect to depth remains constant in the volume considered. All the other parameters become weak functions of time after steady-state heat flow is reached. With appropriate assumptions, Eqs. A-3 and A-4 may be combined to yield a simple relationship between the mass-flow rate and temperature difference, which is given by

$$w\ C = (T_f - T_{ei}) \qquad \textbf{(A-5)}$$